

Structure of $f_0(980)$ from a Coupled Channel Analysis of S -wave $\pi\pi$ Scattering

M.P. LOCHER, V.E. MARKUSHIN AND H.Q. ZHENG

Paul Scherrer Institute, 5232 Villigen PSI, Switzerland

August 27, 1997

Abstract

A coupled channel model is used to study the nature of the $f_0(980)$ resonance. It is shown that the existence of two poles close to $K\bar{K}$ threshold, as found in many data fits and confirmed here, can be reconciled with the $K\bar{K}$ molecular origin of the $f_0(980)$. Due to a strong coupling between channels the number of the S -matrix poles close to the physical region in the physical case exceeds the number of bare states introduced in the model.

1 Introduction

The channel with the vacuum quantum numbers $J^{PC}I^G = 0^{++}0^+$ has several resonances [1] the structure of which has been under discussion for a long time. Recently this problem attracted new attention after a candidate for the scalar glueball was found at LEAR [2, 3]. A characteristic feature of the $J^{PC}I^G = 0^{++}0^+$ channel is that the mixing between different states is strong, so that a connection between the observed resonances and bare states, like quarkonia or glueballs, is nontrivial [4, 5].

In this paper we shall discuss a part of this problem concerned mainly with the $f_0(980)$ resonance. This resonance (the present average values [1] for the mass and width are: $m_{f_0} = 974.1 \pm 2.5$ MeV, $\Gamma_{f_0} = 47 \pm 9$ MeV) has a long history of experimental and theoretical studies. The small width and proximity to the $K\bar{K}$ threshold are among its interesting features, and different explanations have been suggested. We list the most prominent ones. A cryptoexotic $qq\bar{q}\bar{q}$ state was considered in the quark bag model [6]. A $K\bar{K}$ molecular state was found in the potential quark model [7, 8, 9]. A complicated interplay between S -matrix poles and the $K\bar{K}$ threshold structure was shown in [10] to play an important role and obscure conventional simple correspondence between the poles and resonances. The phenomenological analysis in the K-matrix framework favoured for a long time a conventional Breit-Wigner resonance interpretation (contrary to a $K\bar{K}$ state) [11, 12, 13, 14]. A quasi-bound $K\bar{K}$ state was found in the coupled channel models [15, 16, 17] and in the meson exchange interaction model [18, 19]. An exotic vacuum scalar state was considered in [20]. A mixture of a $q\bar{q}$ state and

a scalaron weakly coupled to the $K\bar{K}$ channel was discussed in [21], and a state strongly coupled to the $s\bar{s}$ and $K\bar{K}$ channels near the $K\bar{K}$ threshold was found in the unitarized quark model [4, 22]. A state dominated by the $K\bar{K}$ channel was found in a coupled-channel model derived from the lowest order chiral Lagrangian [23]. For a more complete list of references dealing with the nature of the $f_0(980)$ see [4, 9, 12, 24].

In this paper we shall show that some of the apparently contradicting interpretations of the $f_0(980)$ resonance represent in fact only a part of the multifaceted picture of this state resulting from strong coupling between different channels. In particular, we revise the conventional claim about the connection between the number of poles near the $K\bar{K}$ threshold and the nature of the state ($K\bar{K}$ molecular state vs. coupled channel resonance, see the discussion in [25] and references therein).

Our approach is based on a coupled channel model for the $\pi\pi$ and $K\bar{K}$ systems. Despite of its simplicity it satisfies the minimal requirements which allow an adequate phenomenological description of the $\pi\pi$ scattering amplitudes in the region of the $K\bar{K}$ threshold. Since the solutions are available in analytic form, the trajectories of the S-matrix singularities for coupling constants varied in different ways can be followed explicitly shedding some light on the physical nature of the narrow $f_0(980)$ resonance. A transparent comparison can be made to similar and alternative models in the literature. The model is introduced in Sec. 2, and its parameters are determined from a fit of the $\pi\pi$ scattering phases. The analytic structure of the scattering amplitudes is presented as a function of the parameters in Sec. 3. In Sec. 4 the physical properties of the solutions are discussed and a comparison is made to other approaches in the literature, in particular the validity of the models relating the $f_0(980)$ resonance to a weakly bound $K\bar{K}$ state is elucidated. The details of the formalism are collected in the Appendix.

2 The $\pi\pi - K\bar{K}$ Coupled Channel Model

In order to describe the interaction in the $\pi\pi - K\bar{K}$ system, we introduce a simple model with three channels (here and below we consider the partial wave $J = 0^{++}$ $I^G = 0^+$). Channels 1 and 2 correspond to the $\pi\pi$ and $K\bar{K}$ systems. Channel 3 consists of a bound state in the $|q\bar{q}\rangle$ channel, and the rest of the dynamics in this channel is ignored.

The T -matrix, as a function of the invariant mass squared s , is defined by the Lippmann-Schwinger equation

$$T(s) = V + VG^0(s)T \tag{1}$$

where $G^0(s)$ is the free Green function

$$G^0(s) = \begin{pmatrix} G_1^0(s) & 0 & 0 \\ 0 & G_2^0(s) & 0 \\ 0 & 0 & G_3^0(s) \end{pmatrix} \quad (2)$$

The free Green functions for the $\pi\pi$, $K\bar{K}$, and $q\bar{q}$ channels have the form

$$G_1^0(s) = \frac{2}{\pi} \int_0^\infty \frac{|k_1\rangle\langle k_1|}{s/4 - (m_\pi^2 + k_1^2)} k_1^2 dk_1 \quad (3)$$

$$G_2^0(s) = \frac{2}{\pi} \int_0^\infty \frac{|k_2\rangle\langle k_2|}{s/4 - (m_K^2 + k_2^2)} k_2^2 dk_2 \quad (4)$$

$$G_3^0(s) = \frac{|q\bar{q}\rangle\langle q\bar{q}|}{s - M_r^2} \quad (5)$$

Here $|k_1\rangle$ and $|k_2\rangle$ denote the free $\pi\pi$ and $K\bar{K}$ states with relative momenta k_1 and k_2 , respectively. The state $|q\bar{q}\rangle$ in channel 3 has a bare mass M_r .

To describe the interaction we use the following potential matrix:

$$V = \begin{pmatrix} V_{\pi\pi} & V_{\pi\pi-K\bar{K}} & V_{\pi\pi-q\bar{q}} \\ V_{K\bar{K}-\pi\pi} & V_{K\bar{K}} & V_{K\bar{K}-q\bar{q}} \\ V_{q\bar{q}-\pi\pi} & V_{q\bar{q}-K\bar{K}} & 0 \end{pmatrix} \quad (6)$$

We assume that the diagonal interaction $V_{K\bar{K}}$ produces a bound state in the $K\bar{K}$ channel in the absence of any coupling to the other channels in our model, thus simulating a ‘molecular origin’ of the $f_0(980)$ resonance¹. A strong coupling of this state to the $\pi\pi$ channel is induced by the interaction $V_{\pi\pi-K\bar{K}} = V_{K\bar{K}-\pi\pi}^+$. The $\pi\pi$ channel is assumed to have a strong coupling to the $q\bar{q}$ resonance as well. The $q\bar{q}$ state is also directly coupled to the $K\bar{K}$ channel by the interaction $V_{K\bar{K}-q\bar{q}} = V_{q\bar{q}-K\bar{K}}^+$. The diagonal potential $V_{\pi\pi}$ is used to provide a correct description of the $\pi\pi$ scattering at low energies (see below).

The interaction potentials are taken in separable form:²

$$V = \begin{pmatrix} g_{11}|1\rangle\langle 1| & g_{12}|1\rangle\langle 2| & g_{13}|1\rangle\langle q\bar{q}| \\ g_{12}|2\rangle\langle 1| & g_{22}|2\rangle\langle 2| & g_{23}|2\rangle\langle q\bar{q}| \\ g_{13}|q\bar{q}\rangle\langle 1| & g_{23}|q\bar{q}\rangle\langle 2| & 0 \end{pmatrix} \quad (7)$$

We shall use the following form factors in channel 1 and 2:

$$\langle k|1\rangle = \xi_1(k) = \frac{\mu^{3/2}}{k^2 + \mu_1^2} \quad (8)$$

$$\langle k|2\rangle = \xi_2(k) = \frac{\mu^{3/2}}{k^2 + \mu_2^2} \quad (9)$$

¹The effective interaction in the $K\bar{K}$ channel was demonstrated to be attractive in various quark models [4, 7, 8].

²For our purpose the first rank is sufficient to generate the singularities needed.

where the parameters μ_1 and μ_2 describe the interaction range in the $\pi\pi$ and $K\bar{K}$ channels.

With this choice of the form factors the matrix elements of the Green functions are

$$\langle n|G_n^0(s)|n\rangle = \frac{\mu_n^2}{2(k_n(s) + i\mu_n)^2} \quad , \quad n = 1, 2 \quad (10)$$

where $k_n(s)$ is the relative momentum in the channel n :

$$k_1(s) = \sqrt{s/4 - m_\pi^2} \quad (11)$$

$$k_2(s) = \sqrt{s/4 - m_K^2} \quad . \quad (12)$$

For our model the analytical solution for the T -matrix can be easily obtained. The $\pi\pi$ scattering amplitude $f_{\pi\pi}(s)$ has the form:

$$f_{\pi\pi}(s) = -\langle k_1|T(s)|k_1\rangle = -\frac{\lambda(s)\xi(k_1)^2}{1 - \lambda(s)\langle\xi|G_1^0(s)|\xi\rangle} \quad (13)$$

where

$$\lambda(s) = g_{11} + g_{13}^2 G_3(s) + \frac{(g_{12} + g_{13}g_{23}G_3(s))^2 \langle 2|G_2^0(k_2)|2\rangle}{1 - (g_{22} + g_{23}^2 G_3(s)) \langle 2|G_2^0(k_2)|2\rangle} \quad (14)$$

$$G_3(s) = \frac{1}{s - M_r^2} \quad (15)$$

The first term on the r.h.s. of (14) results from the diagonal interaction in the $\pi\pi$ channel, the second and third terms correspond to the effective interactions induced in the $\pi\pi$ channel by the couplings to the $q\bar{q}$ and $K\bar{K}$ channels. We use the coupling constant g_{11} to satisfy the Adler condition [26], that leads to the vanishing partial wave amplitude at $s = m_\pi^2/2$, by imposing the following constraint

$$\lambda(m_\pi^2/2) = 0 \quad . \quad (16)$$

The connection between the partial wave S -matrix and the scattering amplitude $f_{\pi\pi}$ is given by

$$S_{J=0}^{I=0}(s) = \eta_0^0(s)e^{2i\delta_0^0(s)} = 1 + 2ik_1 f_{\pi\pi}(s) \quad (17)$$

where $\delta_0^0(s)$ is the scattering phase and $\eta_0^0(s)$ is the elasticity parameter.

Considering the coupling constants g_{22} , g_{12} , g_{13} , g_{23} , the interaction ranges μ_1 , μ_2 and the position of the bare $q\bar{q}$ resonance M_r as free parameters, we fitted the $\pi\pi$ scattering amplitude³ from [27, 28, 29] in the energy range $2m_\pi <$

³For a recent discussion of the $\pi\pi$ scattering amplitude see [17, 30].

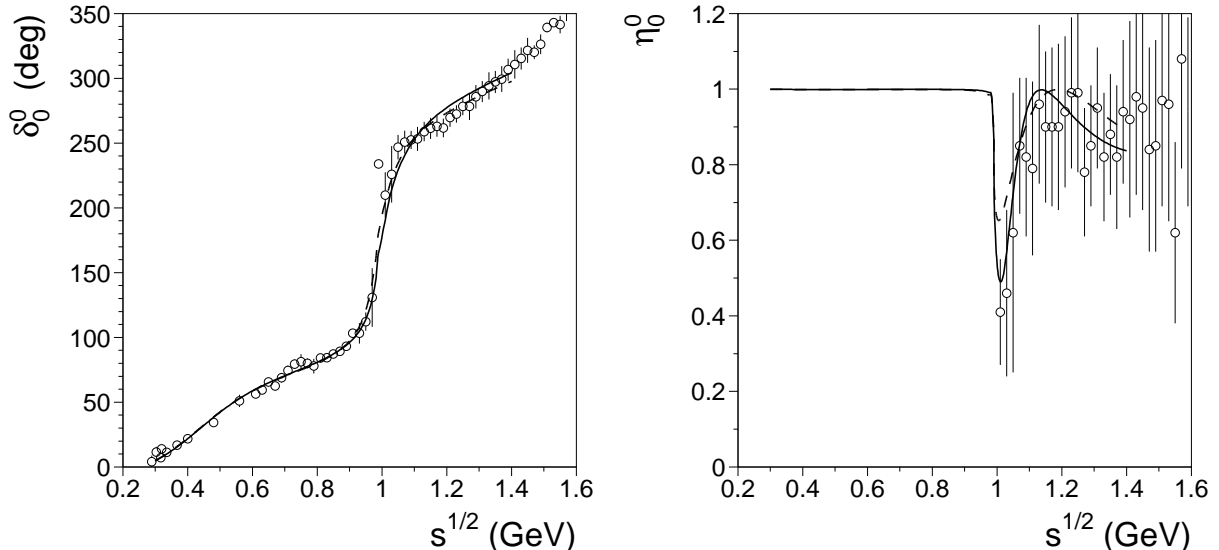


Figure 1: The scattering phase δ_0^0 and the elasticity parameter η_0^0 for the S -wave $\pi\pi$ scattering vs. \sqrt{s} . The curves are our model (the dashed line — fit 1, the solid line — fit 2), the experimental points are from [27, 28, 29].

$\sqrt{s} < 1.4$ GeV. In fitting the $\pi\pi$ scattering data we found a significant correlation between the model parameters, in particular, between the coupling constants and the interaction ranges, so that it was possible to impose some extra constraints preserving a good quality of the fit. The fit 1 (see Fig.1 and Table 1) was done assuming equal interaction ranges ($\mu_1 = \mu_2$) and switching off the direct coupling between the $q\bar{q}$ and $K\bar{K}$ channels ($g_{23} = 0$). A good fit of the $\pi\pi$ scattering data does not automatically lead to a good fit of the $K\bar{K}$ scattering (see Fig.2). However fitting the $\pi\pi$ and $K\bar{K}$ scattering data together we get a fair description of the $K\bar{K}$ phase shift as well (see the fit 2 in Figs.1,2 and Table 1). The calculated S -wave $K\bar{K}$ scattering phase shown in Fig.2 has an energy behaviour typical for the presence of a weakly bound state. The two fits shown represent typical results obtained with our model. Because of a significant uncertainty in the data near the $K\bar{K}$ threshold⁴ and the importance of higher resonances which are not considered here we shall use both sets of the model parameters in the further analysis, the fit 2, however, appears to be preferable.

⁴For a discussion of constraining the $\pi\pi - K\bar{K}$ scattering amplitude by extending the set of experimental data, see [11, 12, 13, 19].

Table 1: The model parameters obtained from the fit. The g_{11} value is calculated using Eq.(16), $m_\pi = 0.1396$ GeV, $m_K = 0.4937$ GeV.

fit	g_{22}	g_{12}	g_{13} GeV	g_{23} GeV	μ_1 GeV	μ_2 GeV	M_r GeV	g_{11}
1 ^a	-5.5332	3.9456	0.69642	0	0.37909	0.37909	1.0916	4.7499
2 ^b	-3.2421	1.9814	0.69358	0.06828	0.3730	0.89975	1.0925	4.6416

(^a) The fit of the δ_0^0 using $g_{23} = 0$, $\mu_1 = \mu_2$.

(^b) Including the fit of the η_0^0 and the $K\bar{K}$ scattering data, μ_1 is fixed.

3 The Poles of the S -Matrix

3.1 The Analytical Structure of the S -Matrix

The Riemann surface of the scattering amplitude for the two channel problem has four sheets due to the kinematical cuts starting at the $\pi\pi$ and $K\bar{K}$ thresholds according to Eqs.(11,12), as shown in Fig.3. The sheets of the complex s -plane are distinguished by the signs of the imaginary parts of the channel momenta k_1 and k_2 , with the standard notation given in Table 2. The physical scattering region corresponds to the upper side of the cut going along the real s axis on the sheet I. If there exist true bound states in both channels, they occur on the sheet I on the real s -axis below all the thresholds. The sheet II accommodates the states which appear as resonances in the channel 1 ($\pi\pi$) and (quasi) bound states in channel 2 ($K\bar{K}$). The sheet III corresponds to resonances in both channels.

Table 2: The sheets of the Riemann surface of the scattering amplitude in the s -plane.

Sheet	Im k_1	Im k_2
I	+	+
II	-	+
III	-	-
IV	+	-

Using our model we found the position of the poles of the S -matrix in the complex s -plane, the result being shown in Table 3. There are two poles, s_A^{II} and s_D^{III} , very close to the $K\bar{K}$ threshold. Another pair of poles, s_B^{II} and s_E^{III} , corresponds to a broad resonance above the $K\bar{K}$ threshold, and the pole s_C^{II} corresponds to a broad structure associated with the $\pi\pi$ threshold. The physics of these poles will be discussed in detail in Sec.3.2. The position of the resonance

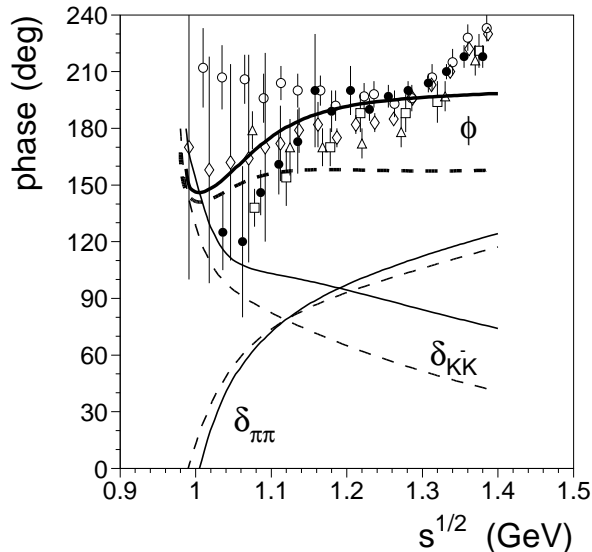


Figure 2: The phase shift $\phi = (\delta_{\pi\pi} + \delta_{K\bar{K}})$ of the $I = 0$ S -wave scattering $\pi\pi \rightarrow K\bar{K}$. The results of our model are shown by the thick lines (fit 1 — dashed, fit 2 — solid). The data are from [31] (\diamond), [32] (\square), [33] (\circ), [34] (\triangle), [35] (\bullet). The phase shifts for the elastic S -wave $I = 0$ $\pi\pi$ and $K\bar{K}$ scattering (modulo 180°) are shown by the thin lines (fit 1 — dashed, fit 2 — solid).

poles depends on the coupling constants, and this distinguishes them from the fixed poles originating from the singularities of the form factors (9). The latter are located at $k_1 = \pm i\mu_1$ and $k_2 = \pm i\mu_2$, their proximity to the physical region being determined by the range of the interaction. In our model these fixed poles approximate the potential singularities which correspond to the left hand cut in a more general case.

3.2 Trajectories of the Resonance Poles

To understand the origin and the nature of the resonance poles found in our model we investigate how these poles move in the complex s -plane when the model parameters are varied between the physical case and the limit of vanishing couplings between the $\pi\pi$, the $K\bar{K}$, and the $q\bar{q}$ channels: $g_{12} = g_{13} = 0$. In this case the diagonal interaction in the $K\bar{K}$ channel with the *physical* strength of the coupling g_{22} produces a bound state close to the $K\bar{K}$ threshold with mass $m_{K\bar{K}} = 0.85$ GeV (for the fit 2 the coupling with the $q\bar{q}$ channel contributes 8 MeV to the binding energy). The $q\bar{q}$ state in the absence of coupling to the open channels is characterized by the mass M_r and zero width.

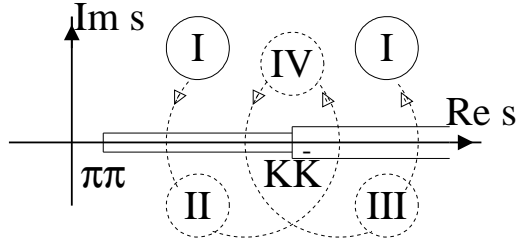


Figure 3: The Riemann surface of the scattering amplitude.

Table 3: The resonance poles of the S -matrix in the s -plane (GeV^2).

Pole	Sheet	fit 1	fit 2
A	II	$0.979 - i0.065$	$1.015 - i0.054$
B	II	$1.653 - i1.163$	$1.521 - i1.092$
C	II	$0.135 - i0.180$	$0.131 - i0.178$
D	III	$1.007 - i0.158$	$1.072 - i0.193$
E	III	$1.562 - i1.773$	$1.207 - i1.696$

The trajectories of the S -matrix poles were calculated for the coupling constants g_{12} and g_{13} varied between zero and the physical values given in Table 1:

$$\begin{aligned}
 g_{12} &\rightarrow x^{1/2} g_{12} , \\
 g_{13} &\rightarrow x^{1/2} g_{13} , \quad 0 \leq x \leq 1
 \end{aligned}
 \tag{18}$$

Figures 4 and 5 display the trajectories plotted in the complex planes of the channel momenta k_1 and k_2 . The four sheets of the complex s -plane correspond to two sheets of the complex momenta planes. Figure 4 shows the k_1 plane that contains the sheets I and II of the s -plane (the second sheet of the k_1 plane, which is not shown here, is reached across the cut going from the $K\bar{K}$ threshold to infinity). All four sheets of the s -plane can be displayed on a single sheet of the k_2 plane with the kinematical cuts going from the $\pi\pi$ thresholds to infinity, as shown in Figure 5. The second sheet in the k_2 plane is a mirror copy (with respect to the imaginary k_2 axis) of the plotted one due to the symmetry properties of the S -matrix [36].

There are three poles on the sheet II. The pole trajectories for the fits 1 and 2 shown in Fig.4 demonstrate two different cases of interplay between the original $K\bar{K}$ bound state and the $q\bar{q}$ resonance. For the fit 1, the pole s_A^I originates from the bound $K\bar{K}$ state and develops an imaginary part due to the coupling to the $\pi\pi$ channel, see the trajectory $(b - S_A^I)$ in Figs.4a,5a. This pole remains, however, close to the $K\bar{K}$ threshold and does not go far away from the real k_1 axis. This occurs because of its interplay with the pole s_B^I which belongs to the trajectory

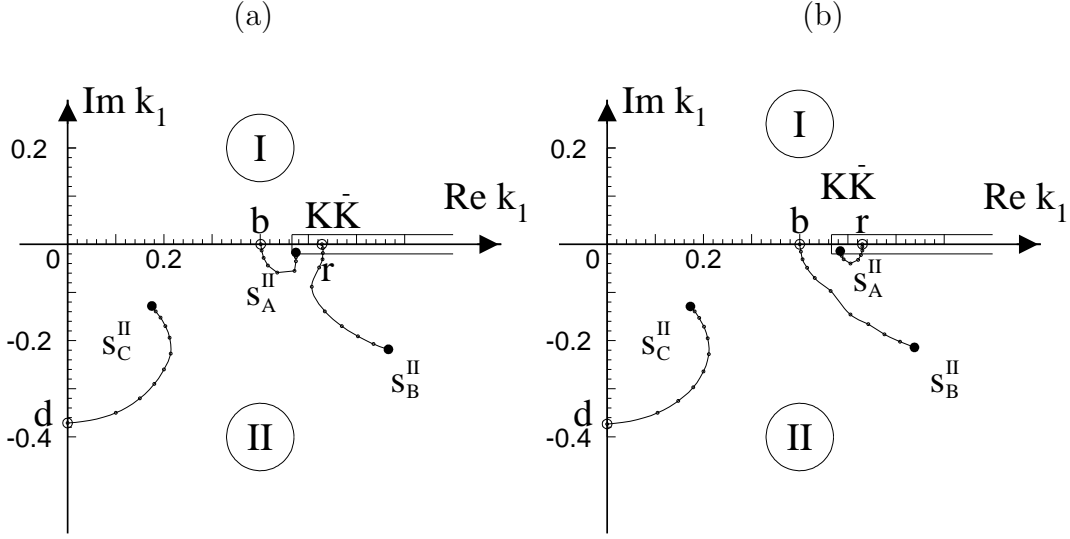


Figure 4: The trajectories of the poles in the complex k_1 plane for the $K\bar{K} - \pi\pi$ and $q\bar{q} - \pi\pi$ couplings increasing from $x = 0$ (\circ) to the physical values $x = 1$ (\bullet). The labels indicate the original positions of the bound state (b), the $q\bar{q}$ resonance (r), and the dynamical pole (d). The dots on the trajectories mark the increase of x in steps of 0.1. Fit 1 is shown in Fig.(a), fit 2 in Fig.(b).

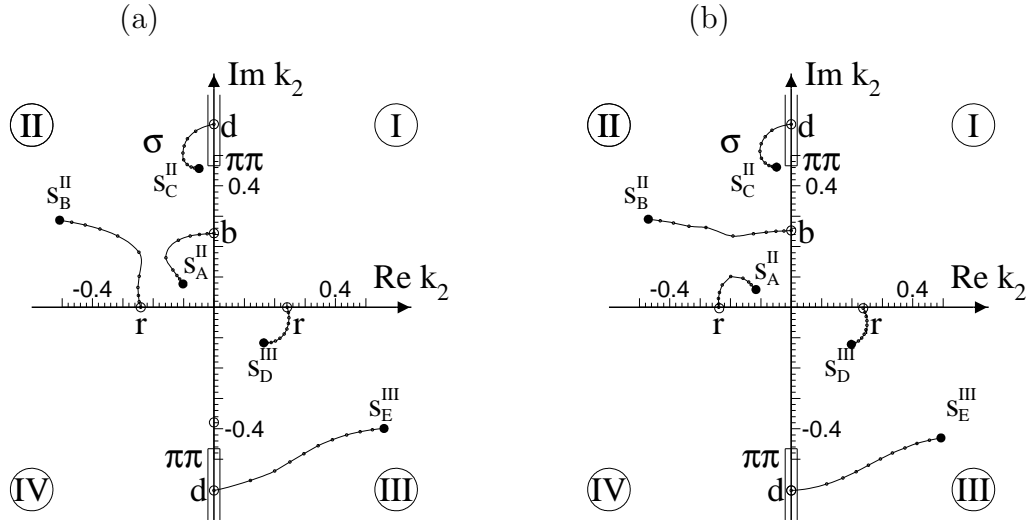


Figure 5: The trajectories of the poles in the complex k_2 plane for the $K\bar{K} - \pi\pi$ and $q\bar{q} - \pi\pi$ couplings increasing from 0 (\circ) to the physical values (\bullet). Fit 1 is shown in Fig.(a), fit 2 in Fig.(b). The labels are as in Fig.4.

$(r - s_B^{II})$ originating from the $q\bar{q}$ state. At small nonzero couplings (18) these two poles develop comparable imaginary parts. With increasing coupling the two poles first get closer but then they start to move away from each other. As a result the pole s_B^{II} gets a large imaginary part while the pole s_A^{II} turns back to the real axis. This kind of pole motion is one of the generic possibilities occurring in the problem of two states coupled via a continuum as discussed in the Appendix.

The fit 2 corresponds to the second generic possibility when the pole originating from the $q\bar{q}$ resonance is attracted to the $K\bar{K}$ threshold producing the narrow state (see the trajectory $(r - s_A^{II})$ on Figs.4b,5b) while the pole originating from the $K\bar{K}$ bound state develops a large width due to the strong coupling to the $\pi\pi$ channel. In both cases the strong attractive interaction in the $K\bar{K}$ channel is essential for the appearance of the pole on the sheet II close to the $K\bar{K}$ threshold.

In both cases the pole s_C^{II} is generated *dynamically* by the effective attractive interaction in the $\pi\pi$ channel resulting from the coupling to the closed channels. The dynamical nature of this pole is seen from the fact that its trajectory $(d - S_C^{II})$ begins at the singularity of the form factor $\xi(k_1)$ at $k_1 = -i\mu_1$. This very broad resonance is responsible for the strongly attractive $\pi\pi$ scattering phase between the $\pi\pi$ and $K\bar{K}$ thresholds and can be associated with the σ meson found in other models [4, 16, 17, 19, 22, 23, 37, 38, 39]. The mass and the width of the σ meson is obtained using the pole position, $s_C^{II} = (M_\sigma - i\Gamma_\sigma/2)^2$, the fits 1 and 2 give similar results: $M_\sigma \approx 0.42$ GeV and $\Gamma_\sigma \approx 0.42$ GeV.

The sheet III contains two pole trajectories showing a similar behaviour in both cases. The $q\bar{q}$ state, being a genuine coupled channel resonance, corresponds to two poles (in the zero coupling limit they are symmetric with respect to the imaginary k_2 axis), see Fig.5. The pole on the sheet II was considered above. The pole on the sheet III moves along the trajectory $(r - s_D^{III})$ closer to the $K\bar{K}$ threshold with increasing coupling to the open channels. For the fit 1, at the physical values of the coupling constants the pole s_D^{III} positions itself *seemingly* as a partner of the pole s_A^{II} with *small* imaginary part, while, by its origin, the pole s_D^{III} is a counterpart of the pole s_B^{II} , as is clearly seen in the weak coupling regime. For the fit 2, the poles moving along the trajectories originating from the initial $q\bar{q}$ poles, $(r - s_A^{II})$ and $(r - s_D^{III})$, look like counterparts for all values of the channel coupling constant between zero and the physical value. The attractive $K\bar{K}$ interaction is essential for keeping these poles close to the $K\bar{K}$ threshold, which again speaks for the $K\bar{K}$ nature of the $f_0(980)$. This result illustrates that on the basis of the physical location of the poles alone the nature of the resonances in strong coupling limit cannot be determined reliably. The study of the *trajectories* in a model can be helpful for uncovering the underlying dynamics.

The pole s_E^{III} on the sheet III has a very large imaginary part, thus it looks like a counterpart of the pole s_B^{II} on the sheet II, as expected for the broad $q\bar{q}$ state strongly coupled to the open channels. However, this naive interpretation cannot be correct because the pole originating from the $q\bar{q}$ state on the sheet III was found to be attracted to the $K\bar{K}$ threshold and has a small width. Figure

5 shows that the pole s_E^{III} has a dynamical origin: the corresponding trajectory emerges from the dynamical singularity of the effective attractive potential in the $\pi\pi$ channel ($k_1 = -i\mu_1$). This result holds for both fits.

The existence of nearby resonance poles of the S-matrix which are 'far away' in the limit of zero channel coupling is a characteristic feature of coupled channel models with potential (left hand) singularities. That is why the coupled channel model can provide a picture of the pole trajectories different from the standard K-matrix parametrization where no poles are generated dynamically, such that all poles must be introduced explicitly.

The interaction between the $K\bar{K}$ bound state and the $q\bar{q}$ state is important for producing the narrow $f_0(980)$ resonance. This can be illustrated by comparing the pole trajectories in Fig.4 with the ones calculated for the cases when either the $K\bar{K}$ or the $q\bar{q}$ channel is switched off, see Fig.6. If the $q\bar{q}$ state is coupled only to the $\pi\pi$ channel, then at the physical strength of the coupling g_{13} the resonance originating from the $q\bar{q}$ state has a width of about 330 MeV, $s_r = (0.96 - i0.33) \text{ GeV}^2$. If the $K\bar{K}$ channel is coupled only to the $\pi\pi$ channel, then the $K\bar{K}$ state at the physical strength of the coupling g_{12} has a width of about 300 MeV, $s_b = (0.39 - i0.19) \text{ GeV}^2$. In both cases an additional very broad resonance with a width of about 1 GeV arises from the dynamical singularity as a result of the strong coupling between the channels.

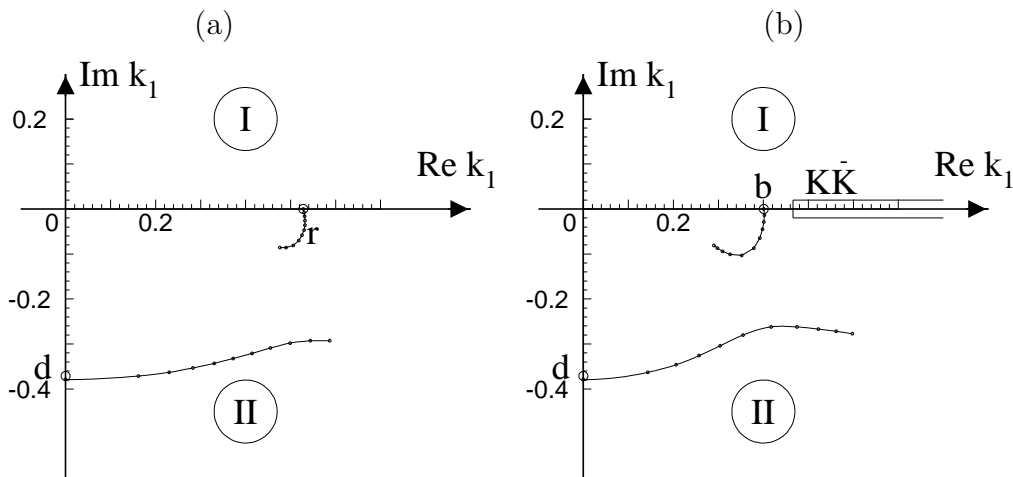


Figure 6: The trajectories of the poles in the complex k_1 plane when one of the channels is switched off: (a) the $q\bar{q}$ state is coupled only to the $\pi\pi$ channel ($g_{12} = g_{22} = 0$); (b) the $\pi\pi$ and $K\bar{K}$ channels are coupled to each other without coupling to the $q\bar{q}$ state ($g_{13} = 0$), all other parameters correspond to the fit 1. The labels are as in Fig.4.

4 Discussion

In this section we discuss how our results are related to previous studies in the literature. In our model the final configuration representing the data has a *pair* of poles close to the $K\bar{K}$ threshold. The pole s_A^{II} on sheet II corresponds to a strong interplay between the original $K\bar{K}$ bound state and the $q\bar{q}$ resonance, the attractive $K\bar{K}$ interaction being important for its proximity to the threshold. Both generic possibilities of the interaction between two poles (see Appendix A) were found to be consistent with the $\pi\pi$ scattering data. When our model is constrained by the $\pi\pi - K\bar{K}$ scattering data, the rearrangement situation is favoured (fit 2): with increasing coupling to the $\pi\pi$ channel the pole originating from $K\bar{K}$ (molecular) bound state nearly collides with the one originating from the $q\bar{q}$ state and then it is repelled and develops a large imaginary part while the pole originating from the $q\bar{q}$ state is attracted to the $K\bar{K}$ threshold. However the alternative situation (fit 1), when the pole s_A^{II} belongs to the trajectory originating from the $K\bar{K}$ bound state, can be realized with relatively small variation of the model parameters and thus is as well a viable solution.

Next in importance by distance to the physical region is the pole s_D^{III} on sheet III, which arises from the $q\bar{q}$ resonance strongly coupled to the $\pi\pi$ and $K\bar{K}$ channels. The remote pole s_B^{II} on the sheet II has a dynamical counterpart s_E^{III} with large width, the latter is created by the interaction between the $q\bar{q}$ state and the $\pi\pi$ channel on sheet III.

This configuration of the poles is similar to the result found for the fits in the K-matrix formalism [11, 12]. The existence of *two* poles close to the $K\bar{K}$ threshold was often interpreted as an evidence against the $K\bar{K}$ molecular state origin of the $f_0(980)$ resonance. While in the limit of weak coupling to the $\pi\pi$ channel the $K\bar{K}$ bound state is clearly described by a single pole, the situation can be very different in the case of strong coupling as our model explicitly demonstrates.

It was found in [12] that the amplitude in the $K\bar{K}$ molecular model of the $f_0(980)$ [9] has only one pole near the $K\bar{K}$ threshold. This, however, does not mean that any other model with the $K\bar{K}$ weakly bound state has the same feature, and our model is just a counterexample. As demonstrated in [12], the fits, which allow two poles near the $K\bar{K}$ threshold, describe the data much better than an one-pole fit. Because in our model the number of the resonance poles is not limited by the number of the bare states, the second pole needed for the best fit to the data is generated dynamically and the overall picture is similar to the favoured two-pole solution in [12].

The exact position of the poles corresponding to the $f_0(980)$ resonance is known to be sensitive to the selection of data used in the fit. Our results concerning the mass and the width of the $f_0(980)$ are compared with some recent results in Table 4 (for detailed description of input data we refer to the original papers).

The dynamical description of the $f_0(980)$ by two poles in our model is similar

Table 4: The of the S -matrix in the \sqrt{s} -plane (GeV) corresponding to the $f_0(980)$ resonance.

Ref.	$M_{f_0} - i\Gamma_{f_0}/2$ (sheet II)	$M_{f_0} - i\Gamma_{f_0}/2$ (sheet III)
fit 1	$0.990 - i0.033$	$1.007 - i0.079$
fit 2	$1.008 - i0.027$	$1.039 - i0.093$
[2]	$0.996 - i0.056$	$0.953 - i0.055$
[4]	$1.006 - i0.017$	
[11] ^a	$1.001 - i0.026$ $0.988 - i0.000$	$0.985 - i0.020$
[12] ^b	$0.988 - i0.024$	$0.978 - i0.028$
[12] ^c	$0.972 - i0.016$	
[13]	$1.008 - i0.043$	$0.957 - i0.041$
[15]	$0.993 - i0.023$	
[16]	$0.973 - i0.029$	
[17] ^d	$0.989 - i0.031$ $0.992 - i0.034$	
[19]	$1.015 - i0.015$	
[21]	$0.987 - i0.040$	$0.967 - i0.069$
[38]	$0.988 - i0.023$	$0.797 - i0.185$
[40]	$0.984 - i0.039$	$0.986 - i0.102$
[41]	$1.015 - i0.043$	

- a) The three-pole fit.
- b) The favoured two-pole fit.
- c) Using the model from [9].
- d) Fits to the “down-flat” and “up-flat” data.

to the result of the unitarized quark model [4] where the strong coupling between the bare quark-antiquark states and the two meson channels was found to produce additional poles. Our model is different from [4] concerning the analytical structure of the transition form-factors, see Eq.(9). In our case the form-factors have poles whose positions are related to the range of interaction. In the model [4] the form-factors are taken in the oscillator form and have an essential singularity at infinity. The shape of the form factors does not seem to be crucial for the quality of fitting the data, but our choice has the advantage of placing the leading dynamical singularities at a finite distance from the thresholds. As both models demonstrate, the interplay between the bare states and the dynamical singularities is important for the correct phenomenological description of the resonances in the scalar-isoscalar channel. An essential feature is that the number of resonance poles can exceed the number of the bare states.

The σ meson is generated dynamically as a broad coupled channel resonance

Table 5: The poles of the S -matrix in the \sqrt{s} -plane (GeV) corresponding to the σ resonance.

Ref.	$M_\sigma - i\Gamma_\sigma/2$ (sheet II)
fit 1	$0.424 - i0.213$
fit 2	$0.420 - i0.212$
[4, 22]	$0.47 - i0.25$
[16]	$0.506 - i0.247$
[17] ^a	$0.518 - i0.261$ $0.562 - i0.233$
[19]	$0.387 - i0.305$
[23]	$0.470 - i0.179$
[37]	$0.460 - i0.338$
[38]	$0.370 - i0.356$
[39]	$0.42 - i0.37$

a) Fits to the “down-flat” and “up-flat” data.

and hence corresponds to a smooth attractive background phase. The parameters of this resonance are expected to be model dependent since the very existence of a broad resonance cannot be proven on the basis of data alone. Our results for the σ are compared with the values from the literature in Table 5.

There is a broad resonance above the $K\bar{K}$ threshold, which is related to the $q\bar{q}$ state strongly coupled with the $\pi\pi$ and $K\bar{K}$ channels, as discussed above. The mass and the width calculated from the position of the poles s_B^{II} and s_E^{III} are $(M_B - i\Gamma_B/2) = (1.36 - i0.43)$ GeV and $(M_E - i\Gamma_E/2) = (1.40 - i0.63)$ GeV (the fit 1). This resonance is similar to that of the K-matrix analysis [12] where a very broad state at about 1 GeV of width around 0.7 GeV was found. In our model this resonance is needed to describe the rise of the $\pi\pi$ scattering phase above the $K\bar{K}$ threshold. It can be considered as an approximation for the higher resonances, in particular, the $f_0(1300)$, and our results for the remote poles s_D^{II} and s_E^{III} should be considered as an estimate rather than the parameters of real physical structures (for the discussion of this energy region see [3, 4, 5, 41, 17, 43] and references therein).

A qualitative description of this mass range would require accounting for additional higher resonances, see [5, 40, 41]. We do not attempt it here, however, we can use our model to demonstrate how the $q\bar{q}$ state dissolves into the continuum. This problem is especially interesting because the channel coupling is strong, such that the poles corresponding to the very broad resonance and the bare state belong to different trajectories (compare the s_E^{III} and the s_D^{III} in Fig.5 in both fits). Our approach is based on the probability sum rule for a resonance

embedded into a continuum [42]. Using the full Green function

$$G(s) = G^0(s)(1 + T(s)G^0(s)) \quad (19)$$

and projecting the completeness relation in channel space onto the $q\bar{q}$ channel one gets

$$\int_{4m_\pi^2}^{\infty} w(s)ds = \langle q\bar{q}|q\bar{q} \rangle = 1 \quad , \quad (20)$$

where

$$w(s) = \frac{1}{2\pi i}(G_3(s - i\epsilon) - G_3(s + i\epsilon)) \quad , \quad (21)$$

$$G_3(s) = \langle q\bar{q}|G(s)|q\bar{q} \rangle = \frac{1}{s - M_r^2 - \Pi(s)} \quad , \quad (22)$$

and $\Pi(s)$ is the mass operator of the $q\bar{q}$ state:

$$\Pi(s) = \frac{4(g_{13}^2 G_1^0(s) + g_{23}^2 G_2^0(s) + (2g_{12}g_{13}g_{23} - g_{13}^2 g_{22} - g_{23}^2 g_{11})G_1^0(s)G_2^0(s))}{1 - g_{11}G_1^0(s) - g_{22}G_2^0(s) + (g_{11}g_{22} - g_{12}^2)G_1^0(s)G_2^0(s)} \quad (23)$$

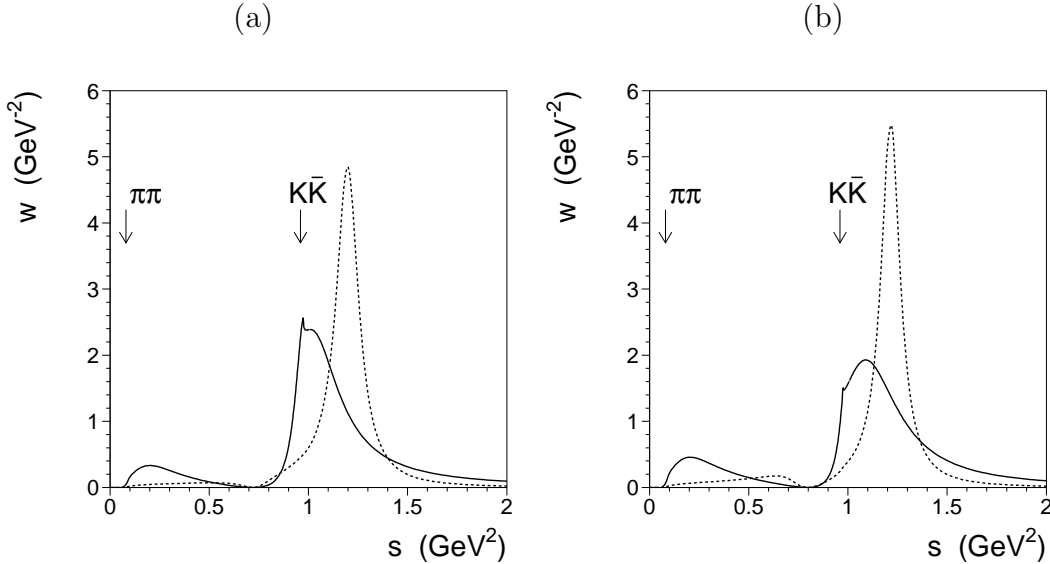


Figure 7: The probability density for the $q\bar{q}$ state embedded in the continuum. The solid line corresponds to the physical parameters, the dashed line is for $x = 0.2$ in Eq.(18): (a) fit 1, (b) fit 2.

According to Eq.(20) the function $w(s)$ determines the probability density for the $q\bar{q}$ component in the scattering states within the interval $(s, s + ds)$, as shown

in Fig.7. In the case of weak coupling the probability density is well localized near the position of the bare $q\bar{q}$ state. For the physical case we find a broad peak centered slightly above the $K\bar{K}$ threshold, so that there is a significant overlap of the $w(s)$ distribution with the $f_0(980)$ resonance. This down shift with respect to the position of the original $q\bar{q}$ state is due to the strong attraction of the s_D^{III} pole towards the $K\bar{K}$ threshold. The position and the width of the $w(s)$ distribution indicates that an essential contribution to the saturation of the sum rule (20) comes from the pole s_D^{III} , while the narrow structure associated with the pole s_A^{II} alone plays a minor role. Thus out of the two poles related to the narrow $f_0(980)$ state only the pole on sheet III has a large $q\bar{q}$ component and the pole on sheet II has mainly $K\bar{K}$ nature.

5 Conclusion

We have re-examined the resonance structures in the $J^{PC}I^G = 0^{++}0^+$ partial wave of $\pi\pi$ scattering below 1 GeV, including the $f_0(980)$ and σ resonances on the basis of an exactly solvable coupled channel model. The model has the following features: a separable diagonal $K\bar{K}$ potential producing a weakly bound state, a separable transition potential $V_{\pi\pi-K\bar{K}}$ (representing K^* -exchange, e.g.) which couples the $\pi\pi$ and $K\bar{K}$ channels, and a broad resonance in the $q\bar{q}$ channel which represents background and is coupled to the $\pi\pi$ and $K\bar{K}$ channels. Tuning the model parameters the experimental energy dependence of the $\pi\pi$ S -wave scattering phase $\delta_0^{I=0}(s)$ is reproduced accurately. The interpretation of the singularities is elucidated by tracing the trajectories of the S -matrix poles as a function of the strength of the channel couplings. Two generic cases are represented by fit 1 and fit 2.

In our model the $f_0(980)$ resonance corresponds to two S -matrix poles close to the $K\bar{K}$ threshold. The pole on sheet II (s_A^{II}) corresponds to the interplay between the original $K\bar{K}$ (molecular) bound state and the $q\bar{q}$ state due to their coupling via the $\pi\pi$ channel. This pole has many features typical for the $K\bar{K}$ bound state in the absence of the coupling to the $\pi\pi$ channel. The model parameters consistent with the data allow two possibilities when the coupling with the $\pi\pi$ channel is switched on: the pole s_A^{II} originates either directly from the $K\bar{K}$ bound state (fit 1) or through the rearrangement from the $q\bar{q}$ state colliding with the $K\bar{K}$ state (fit 2). The second pole on sheet III (s_D^{III}) arises from the $q\bar{q}$ resonance coupled to the $\pi\pi$ and $K\bar{K}$ channels. It has a large $q\bar{q}$ component, but its position close to the $K\bar{K}$ threshold is due to the attractive interaction in the $K\bar{K}$ channel. There is no contradiction between the presence of two poles close to $K\bar{K}$ threshold and the molecular origin of the $f_0(980)$ resonance.

The remote poles on sheet II (s_B^{II}) and sheet III (s_E^{III}) correspond to a smooth background phase, the latter originates from the dynamical singularity describing the coupling of the $q\bar{q}$ resonance to the $\pi\pi$ channel. The σ meson is generated

dynamically by the strong coupling $q\bar{q} \leftrightarrow \pi\pi$ resulting in an effective attractive interaction in the $\pi\pi$ channel below the $q\bar{q}$ state (s_C^{II}). The appearance of dynamical coupled channel poles is a crucial feature; in the physical case the number of poles close to the physical region exceeds the number of bare states in the model.

Overall the resulting configuration is similar to the results from the phenomenological K-matrix analysis: two poles close to the $K\bar{K}$ threshold. Our model shows that the interpretation of the scattering data is entirely consistent with a $K\bar{K}$ state picture for the f_0 resonance, which is thus not in conflict with the (phenomenological) requirement of having two poles (not one) near the $K\bar{K}$ threshold.

Acknowledgments

We thank M.R. Pennington for comments on the nature of the $f_0(980)$ and L. Leśniak for a discussion of the $\pi\pi - K\bar{K}$ scattering data.

Appendix A. Two states coupled via a continuum

Contrary to direct coupling between two states which is well known to result in their repulsion, a coupling of two states via a continuum channel can induce an effective attraction. This problem has been treated in the literature (see, for example, [44]), so here we give only a brief summary for the benefit of the reader.

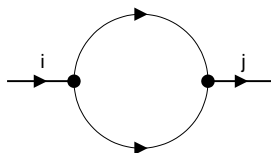


Figure 8: The system of two states ($i, j = 1, 2$) coupled with the continuum channel.

We consider two states with energies E_1^0 and E_2^0 , which are coupled to the continuum channel. This coupling induces an effective interaction described by the mass operators

$$\begin{pmatrix} V_{11} & V_{12} \\ V_{21} & V_{22} \end{pmatrix} = \begin{pmatrix} g_1^2 \langle 1|G(E)|1\rangle & g_1 g_2 \langle 1|G(E)|2\rangle \\ g_1 g_2 \langle 2|G(E)|1\rangle & g_2^2 \langle 2|G(E)|2\rangle \end{pmatrix} \quad (24)$$

where g_i is the coupling between the state i and the continuum, $|i\rangle$ is the corresponding vertex, and $G(E)$ is the Green function of the continuum channel. The

mass operators V_{ij} are energy dependent: in particular, they have kinematical cuts starting from the continuum threshold. When the states 1 and 2 are coupled to the *open* channel, they are not the eigenstates of the full Hamiltonian, but become resonances located on the second sheet, where $\text{Im}V_{ij} \leq 0$, and they can be identified with the poles of the Green function. Their position is determined by the equation

$$\det \begin{pmatrix} E - E_1^0 - V_{11} & V_{12} \\ V_{21} & E - E_2^0 - V_{22} \end{pmatrix} = 0 \quad (25)$$

For the sake of simplicity, we assume the states 1 and 2 to be far above the threshold and neglect the energy dependence of the mass operators. Furthermore we consider only the imaginary parts of the mass operators⁵ and use the following parametrization: $V_{11} = -i\Gamma_1/2$, $V_{12} = V_{21} = -i\sqrt{\Gamma_1\Gamma_2}/2$, $V_{22} = -i\Gamma_2/2$. Equation (25) is then reduced to

$$\det \begin{pmatrix} E - E_1^0 - i\Gamma_1/2 & -i\sqrt{\Gamma_1\Gamma_2}/2 \\ -i\sqrt{\Gamma_1\Gamma_2}/2 & E - E_2^0 - i\Gamma_2/2 \end{pmatrix} = 0 \quad (26)$$

which has the resonance pole solutions:

$$E_{\pm} = \frac{(E_1^0 + E_2^0) - i(\Gamma_1 + \Gamma_2)/2}{2} \pm \frac{1}{2} \sqrt{(E_1^0 - E_2^0 - i\Gamma_1 + i\Gamma_2)^2 - \Gamma_1\Gamma_2} \quad (27)$$

Considering the resonance positions as functions of the individual couplings ($\Gamma_1 \sim g_1^2$, $\Gamma_2 \sim g_2^2$) we find the different types of solutions shown in Fig.9. The trajectories plotted correspond to the solutions E_{\pm} for variable width Γ_1 and fixed values of Γ_2 and the initial positions E_1^0 and E_2^0 . As the width Γ_1 increases starting from zero, the two poles first attract each other, but then the attraction turns into repulsion. There are three different types of solutions for the trajectories $E_{\pm}(\Gamma_1)$, which correspond to the following cases:

$$\begin{aligned} (a) \quad & \Gamma_2 < |E_1^0 - E_2^0| \\ (b) \quad & \Gamma_2 = |E_1^0 - E_2^0| \\ (c) \quad & \Gamma_2 > |E_1^0 - E_2^0| \end{aligned} \quad (28)$$

In the case (a) the trajectory corresponding to the solution $E_-(\Gamma_1)$ remains bounded, as Γ_1 goes to infinity, while in the case (c) the bounded trajectory corresponds to the solution $E_+(\Gamma_1)$. In the case (b) the trajectories collide in the complex plane at $\Gamma_1 = \Gamma_2$. In all cases, infinite growth of Γ_1 does not make both states infinitely broad: there is always a solution with width smaller than $|E_1^0 - E_2^0|$.

⁵The real parts lead to the well known shifts due to the diagonal interactions and to the mutual repulsion due to the nondiagonal interactions.

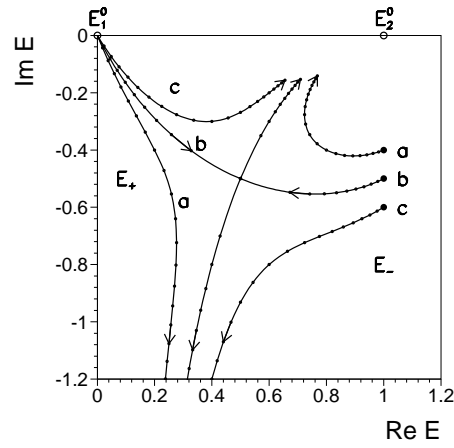


Figure 9: The poles of the Green function in the complex energy plane for the system of two states coupled via a continuum. The trajectories show the motion of the poles as function of Γ_1 for three different cases: (a) $\Gamma_2 = 0.8|E_1^0 - E_2^0|$, (b) $\Gamma_2 = |E_1^0 - E_2^0|$, (c) $\Gamma_2 = 1.2|E_1^0 - E_2^0|$.

References

- [1] Review of Particle Properties, Phys. Rev. D **54** (1996) 1.
- [2] C. Amsler *et al.*, Phys. Lett. B **342** (1995) 433.
- [3] C. Amsler and F.E. Close, Phys. Lett. B **353** (1995) 385; Phys. Rev. D **53** (1996) 295.
- [4] N.A. Törnqvist, Z. Phys. C **68** (1995) 647.
- [5] A.V. Anisovich, V.V. Anisovich, and A.V. Sarantsev, Phys. Lett. B **395** (1997) 123; hep-ph/9702339.
- [6] R.J. Jaffe, Phys. Rev. D **15** (1977) 267.
- [7] J. Weinstein and N. Isgur, Phys. Rev. Lett. **48** (1982) 659; Phys. Rev. D **27** (1983) 588.
- [8] S. Godfrey and N. Isgur, Phys. Rev. D **32** (1985) 189.
- [9] J. Weinstein and N. Isgur, Phys. Rev. D **41** (1990) 2236.
- [10] R.N. Cahn and P.V. Landshoff, Nucl. Phys., **B266** (1986) 451.
- [11] K.L. Au, D. Morgan and M.R. Pennington, Phys. Rev. D **35** (1987) 1633.
- [12] D. Morgan and M. R. Pennington, Phys. Rev. D **48** (1993) 1185.
- [13] A.V. Anisovich and A.V. Sarantsev, Phys. Lett. B **382** (1996) 429.
- [14] A.V. Anisovich, V.V. Anisovich, and A.V. Sarantsev, hep-ph/9702339.
- [15] F. Cannata, J.P. Dedonder, and L. Leśniak, Z. Phys. A **334** (1989) 457; Z. Phys. A **343** (1992) 451.
- [16] R. Kamiński, L. Leśniak, and J.-P. Maillet, Phys. Rev. D **50** (1994) 3145.
- [17] R. Kamiński, L. Leśniak, and B. Loiseau, hep-ph/9707377.
- [18] D. Lohse, J.W. Durso, K. Holinde, and J. Speth, Phys. Lett. B **234** (1990) 235.
- [19] G. Janssen, B.C. Pearce, K. Holinde, and J. Speth, Phys. Rev. D. **52** (1995) 2690.
- [20] V.N. Gribov, Lund preprint LU-TP-91-7, 1991; F.E. Close, Yu.L. Dokshitzer, V.N. Gribov, V.A. Khoze, and M.G. Ryskin, Phys. Lett. B **319** (1993) 291.

- [21] V.V. Anisovich, A.A. Kondrashov, Yu.D. Prokoshkin, S.A. Sadovsky, and A.V. Sarantsev, Phys. Lett. B **355** (1995) 363.
- [22] N.A. Törnqvist and M. Roos, Phys. Rev. Lett. **76** (1996) 1575.
- [23] J.A. Oller and E. Oset, Nucl. Phys. **A620** (1997) 438 .
- [24] A. Palano, Nucl. Phys. B (Proc. Suppl.) **39B** (1995) 287.
- [25] D. Morgan, Nucl. Phys. **A543** (1992) 632.
- [26] S.L. Adler, Phys. Rev. **137B** (1965) 1022; Phys. Rev. **139B** (1965) 1638.
- [27] G. Grayer *et al.*, Nucl. Phys. **B75** (1974) 189.
- [28] W. Ochs, Ph.D. thesis, Munich Univ., 1974.
- [29] L. Rosselet *et al.*, Phys. Rev. D **15** (1977) 574.
- [30] R. Kamiński, L. Leśniak, and K. Rybicki, Z. Phys. C **74** (1997) 79.
- [31] A.D. Martin and E.N. Ozmütlu, Nucl. Phys. **B158** (1979) 520.
- [32] V.A. Polychronakos *et al.*, Phys. Rev. D **19** (1979) 1317.
- [33] D. Cohen *et al.*, Phys. Rev. D **22** (1980) 2595.
- [34] G. Costa *et al.*, Nucl. Phys. **B175** (1980) 402.
- [35] A. Etkin *et al.*, Phys. Rev. D **25** (1982) 1786.
- [36] R.J. Eden and J.R. Taylor, Phys. Rev. **133** (1964) B1575.
- [37] J.L. Basdevant and J. Zinn–Justin, Phys. Rev. D **3** (1971) 1865; D. Iagolnitzer, J. Justin and J. B. Zuber, Nucl. Phys. **B60** (1973) 233.
- [38] B.S. Zou and D.V. Bugg, Phys. Rev. D **48** (1994) R3948; Phys. Rev. D **50** (1994) 591.
- [39] N.N. Achasov and G.N. Shestakov, Phys. Rev. D **49** (1994) 5779.
- [40] V.V. Anisovich, D.V. Bugg, A.V. Sarantsev, and B.S. Zou, Phys. Rev. D **50** (1994) 1972.
- [41] A.V. Anisovich, V.V. Anisovich, Yu.D. Prokoshkin, and A.V. Sarantsev, Phys. Lett. B **389** (1996) 388;
- [42] L.N. Bogdanova, G.M. Hale, and V.E. Markushin, Phys. Rev. C **44** (1991) 1289.

- [43] W.M. Kloet and B. Loiseau, *Z. Phys. A* **353** (1995) 227; nucl-th/9708038.
- [44] A.M. Badalian, L.P. Kok, M.I. Polikarpov, and Yu.A. Simonov, *Phys. Rep.* **82** (1982) 31.